Multiscale 3D Edge Representation of Volume Data by a DOG Wavelet

Shigeru Muraki
Electrotechnical Laboratory

Abstract

This paper proposes a method to expand volume data into the 3D DOG (*Difference of Gaussians*) functions by using the frame theory of non-orthogonal wavelets. The spherically symmetric feature of the 3D DOG function is suitable for the visualization methods based on the volume density projection. Since the DOG function approximates a $\nabla^2 G$ (*Laplacian of Gaussian*) function, the representation can be considered as a hierarchy of the 3D edges on different scales. Therefore we can enhance the edge information at will by blending the projection images on different scales. Since the wavelet coefficients have significant value where the volume density changes, we may use this representation method for the enhancement of the biomedical features and also can use it as a data compression method by neglecting the insignificant coefficients. We will apply our representation method to medical CT volume data and show the efficiency in describing the spatial structure of the volume.

1 Introduction

As the performance of computed tomography (CT) and magnetic resonance (MR) scanners advances, volume data has become widespread in medicine [1]. In the field of computer graphics, various volume visualization methods have been proposed [2]. However, most of them are classified into two classes, the surface rendering strategy [3] and the density projection strategy [4]. In the surface rendering strategy, the geometric model such as the 3D contours of the volume are extracted first, and then rendered by using the conventional polygon rendering technique. However, this strategy represents only a portion of the volume and can not use all of the information which the volume contains. In the density projection strategy, all of the densities of the voxels are projected onto the image plane. However, the overlapping of numerous voxels makes it difficult to show the spatial structure of the volume. Therefore we need to carefully adjust the additional parameters of each voxel, such as the opacity or the color, to enhance the spatial structure of the volume [5].

In this paper we propose a method to expand volume data into the multiscale primitives, i.e., 3D DOG (*Difference of Gaussians*) [6] functions. Although the 3D DOG function is not an orthonormal function, the frame theory of the non-orthogonal wavelets makes the expansion possible [7]. The spherically symmetric feature of the primitives is convenient for the integration of the volume densities along a certain line, therefore the density projection strategy in our representation is much easier than in the voxel representation. Further, the DOG function approximates a $\nabla^2 G$ (*Laplacian of Gaussian*) function [6], which is the popular edge operator in computer vision field, then the representation can be considered to be a hierarchy of 3D edges on different scales. Consequently, we can enhance the spatial structure of the volume at will by blending the projection images on different scales. Since the wavelet coefficients have significant value where the volume density changes, we may use this representation method for the enhancement of the biomedical features and can also use it as a data compression method by neglecting the insignificant coefficients. In the following sections, we apply our representation method to a medical CT volume data and show the efficiency in describing the spatial structure of the volume.

Adderss: 1-1-4 Umezono, Tsukuba, 305 Japan
Phone: +81-298-58-5947
E-mail: muraki@etl.go.jp

0-8186-7067-3/95 $4.00 © 1995 IEEE

2 Non-orthogonal Wavelet

One-dimensional(1D) *wavelet* is a family of functions which is defined by a single *mother wavelet* $\psi(t)$, the dilation parameter a and the shift parameter b as

$$\psi_{a,b} = a^{-1/2}\psi(\frac{t-b}{a}), \quad (a, b \in \mathbf{R}),$$

where $\mathbf{R}$ denotes the set of real numbers. The necessary conditions (*admissibility condition*) for the function $\psi(t)$ are to converge to zero at a long way and to have no DC components. With an appropriate choice of $\psi(t)$, a and b, we can make $\psi_{a,b}$ a *frame* [7] of $L^2(\mathbf{R})$, where $L^2(\mathbf{R})$ denotes the set of measurable and square-integrable 1D functions. The frame is a family of functions for which there exist positive constants A and B, such that

$$A\|f\|^2 \leq \sum_{a,b} |\langle f, \psi_{a,b}\rangle|^2 \leq B\|f\|^2, \tag{1}$$

where the symbol $\langle , \rangle$ denotes the inner product of two $L^2(\mathbf{R})$ functions. A frame $\{\psi_{a,b}\}$ brings with it a *dual frame* $\{\tilde{\psi}_{a,b}\}$ and any $L^2(\mathbf{R})$ function $f(x)$ can be expanded into $\psi_{a,b}$ as

$$f = \sum_{a,b} \langle f, \tilde{\psi}_{a,b}\rangle \psi_{a,b}.$$

Even though the dual frame is difficult to find, if A and B are close to each other, we can closely approximate $f(x)$ by using $\psi_{a,b}$ as

$$f \approx \frac{2}{A+B} \sum_{a,b} \langle f, \psi_{a,b}\rangle \psi_{a,b}, \tag{2}$$

where $(A+B)/2$ is called the *redundancy* of the frame. If the two frame bounds are equal, $A = B$, $\{\psi_{a,b}\}$ is called a *tight frame*. In the special case of $A = B = 1$, the tight frame is an orthogonal basis. Even if A and B are not close to each other, we can expand $f(x)$ into $\psi_{a,b}$ with an iterative technique [7] such as

$$f = \lim_{N \to \infty} f_N, \tag{3}$$

where

$$f_N = f_{N-1} + \frac{2}{A+B} \sum_{a,b} [\langle f, \psi_{a,b}\rangle - \langle f_{N-1}, \psi_{a,b}\rangle] \psi_{a,b}. \tag{4}$$

3 DOG Wavelet and Blobby Object

The author previously described a volume data by an orthogonal 3D wavelet, however the function shape of the wavelet was too complicated to develop the efficient visualization method [9]. In this paper, we renounce the orthogonality and use a 3D DOG (*Difference of Gaussians*) function as a mother wavelet to simplify the visualization. Figure 1 shows an example of 1D DOG function. In the field of computer vision, the DOG function is used to approximate the response of the "receptive field" of human visual neurons. It is also known that the DOG function closely approximates the $\nabla^2 G$ function. Since our aim is to use the DOG function as a primitive form of volume representation, we need to extend the 1D wavelet theory into 3D. There exist several methods to construct multidimensional wavelets: e.g., by using the tensor product of 1D wavelets [8, 9], by using rotation parameters [10] and by using a spherically symmetric wavelet [7]. In this paper we use a spherically symmetric DOG function,

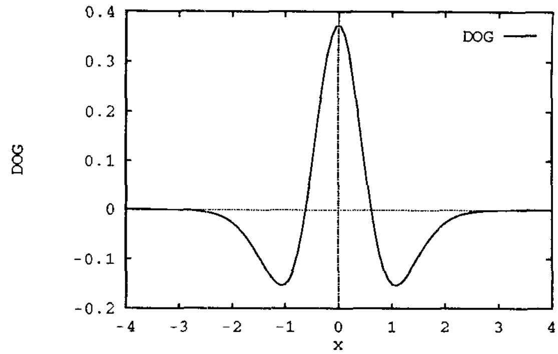

Figure 1: One dimensional DOG function. ($\sigma_1 = 0.70, \sigma_2 = 1.12$).

$$\psi(\vec{\mathbf{x}}) = e^{-|\vec{\mathbf{x}}|^2/\sigma_1^2} - (\frac{\sigma_1}{\sigma_2})^3 e^{-|\vec{\mathbf{x}}|^2/\sigma_2^2}, \tag{5}$$

as a mother wavelet. Equation (5) is equivalent to a pair of Blinn's blobby object [11], which is used to design both a smooth and complicated object in the field of computer graphics. Consequently, by defining a 3D frame

$$\psi_{a,\vec{\mathbf{b}}}(\vec{\mathbf{x}}) = a^{-3/2}\psi(\frac{\vec{\mathbf{x}} - \vec{\mathbf{b}}}{a}), \quad (a \in \mathbf{R}, \vec{\mathbf{x}}, \vec{\mathbf{b}} \in \mathbf{R}^3),$$

with an appropriate choice of a and $\vec{\mathbf{b}}$, we can approximate any volume data V as

$$V \approx \lambda \sum_{a,\vec{\mathbf{b}}} \langle V, \psi_{a,\vec{\mathbf{b}}}\rangle \psi_{a,\vec{\mathbf{b}}} \tag{6}$$

and can obtain the identical representation with the Blinn's blobby object. If we choose $a = 2^l$ ($l \in \mathbf{Z}$), the frame corresponds to a dyadic multiresolution pyramid [8, 9], where $\mathbf{Z}$ denotes the set of integers. And although

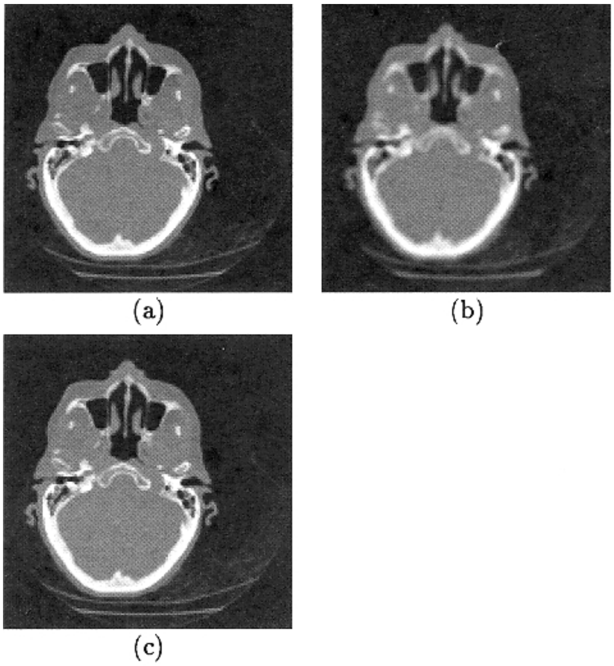

Figure 2: (a) Original CT image. (b) Image reconstructed after one iteration. (c) Image reconstructed after 20 iterations.

there are many ways to locate the shift parameter $\vec{\mathbf{b}}$ in 3D space, the multiresolution lattice,

$$\vec{\mathbf{b}}_{i,j,k,l} = (2^l i, 2^l j, 2^l k), \quad (i,j,k,l \in \mathbf{Z}) \tag{7}$$

will be the most natural selection for cuboidal volume data. Consequently, we define the primitive of each scale parameter l as

$$\psi_l(\vec{\mathbf{x}}) = 2^{-\frac{3}{2}l}\psi(2^{-l}\vec{\mathbf{x}}), \tag{8}$$

and then expand the volume data V into the primitives as

$$V(\vec{\mathbf{x}}) \approx \lambda \sum_{i,j,k,l} \langle V, \psi_l(\vec{\mathbf{x}} - \vec{\mathbf{b}}_{i,j,k,l})\rangle \psi_l(\vec{\mathbf{x}} - \vec{\mathbf{b}}_{i,j,k,l}). \tag{9}$$

The constant λ should be determined from the frame bounds, A and B, as Equation (2). Although Daubetchies [7] showed the method to estimate the frame bounds of 1D wavelets, its extension to 3D is not easy. Therefore we will determine the value of λ by a least square method in the next section.

4 3D DOG Expansion of Volume Data

Figure 2(a) is a slice of a volume data (CThead) of the Chapel Hill Volume Rendering Test Dataset courtesy of University of North Carolina. This volume data consists of 113 slices of 256×256 X-ray CT images. To equalize the resolution in the three directions (width, height and depth), we reduced the size of each image by using Mallat's two-dimensional wavelet transforms [8] and then obtained a volume data V of 128^3 voxels by adding 15 blank images. To expand V into the 3D DOG functions, we need to calculate the continuous inner product

$$\langle V, \psi_l(\vec{\mathbf{x}} - \vec{\mathbf{b}}_{i,j,k,l})\rangle, \tag{10}$$

as in Equation (9). Since V is discrete volume data, we substituted a discrete 3D convolution of V with a 3D kernel, which is the discretization of function ψ_l, for Equation (10). Although the 3D convolution consumes much time in general, the use of a 3D DOG function for ψ_l reduces this time a great deal. Namely, the 3D DOG function is defined by the difference of two 3D Gaussian functions as Equation (5), and each 3D Gaussian function can be separated into the multiplication of three 1D functions as

$$e^{-|\vec{\mathbf{x}}|^2/\sigma^2} = e^{-x^2/\sigma^2} e^{-y^2/\sigma^2} e^{-z^2/\sigma^2} \tag{11}$$

Hence Equation (5) can be substituted by six 1D convolutions and the order of the calculation amount is reduced from M^3 to $6M$, where M denotes the extent of the kernel. For practical calculations, we need to determine the value of σ_1 and σ_2 in Equation (5). Marr et al. reported that a DOG function closely approximates a $\nabla^2 G$ at the ratio of $\sigma_2/\sigma_1 = 1.6$ [6]. Since the purpose of this paper is to describe a volume data with the multiscale 3D edge primitives, we tacitly assume that $\sigma_2 = 1.6\sigma_1$ in this paper.

We expanded the volume data V by using the value $\sigma_1 = 0.7$. The range of the scale parameter we used was $0 \leq l \leq 7$ and the kernel extent M was 9 for $l = 0$ and more for $l > 0$. The total number of the obtained non-zero coefficients was 2,971,734, which was about 1.4 times larger than the number of the voxels of V. The calculation time for the expansion was 6 minutes and 20 seconds on an HP9000/735 workstation. To reconstruct the continuous approximation of V from these coefficients, we need to determine the value of λ in Equation (9). We then generated the discrete volume data V_d', which had the same structure as V, from the continuous volume

$$V'(\vec{\mathbf{x}}) = \sum_{l=0}^{7}\sum_{i,j,k} \langle V, \psi_l(\vec{\mathbf{x}} - \vec{\mathbf{b}}_{i,j,k,l})\rangle \psi_l(\vec{\mathbf{x}} - \vec{\mathbf{b}}_{i,j,k,l}),$$

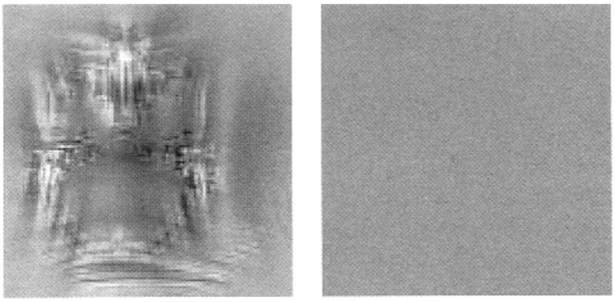

(a) (b)

Figure 3: (a) The difference between Figure 2(b) and 2(a). (b) The difference between Figure 2(c) and 2(a).

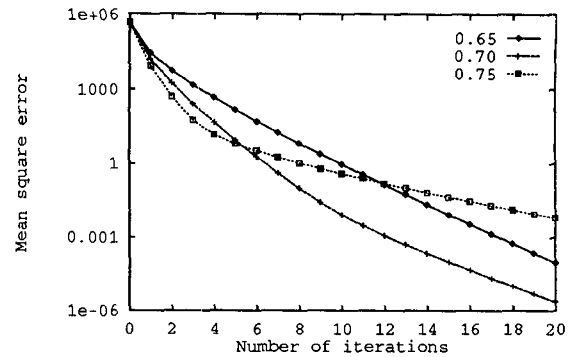

Figure 4: The variations of the mean square errors as the number of iterations increases($\sigma_1 = 0.65, 0.70, 0.75$).

and determined that $\lambda = 0.642$ by solving the least square method,

$$\frac{d\|V - \lambda V_d'\|^2}{d\lambda} = 0. \tag{12}$$

Where the symbol $\|V\|^2$ denotes the squared sum of all of the voxels of V. Figure 2(b) is the same slice of $\lambda V_d'$ as Figure 2(a). Figure 3(a) shows the difference between Figure 2(b) and 2(a). The clear distinction indicates that the approximation of Equation (9) is not sufficient. The reason for the poor quality of the approximation is that Equation (2) can not be considered valid since the frame bounds, A and B, are not close to each other. Although we need the dual frame for the complete expansion, the dual frame is difficult to obtain. In that case, we use the following iterative method to make the expansion possible by referring to Equation (3) and (4).

1. Let $c_{i,j,k,l} = 0$ for every i, j, k, l.
2. Let $c'_{i,j,k,l} = \langle V, \psi_l(\mathbf{x} - \vec{\mathbf{b}}_{i,j,k,l})\rangle$ for every i, j, k, l.
3. Reconstruct $V' = \sum_{l=0}^{7} \sum_{i,j,k} c'_{i,j,k,l}\psi_l(\vec{\mathbf{x}} - \vec{\mathbf{b}}_{i,j,k,l})$ and determine λ by solving Equation (12).
4. Let $c_{i,j,k,l} = c_{i,j,k,l} + \lambda c'_{i,j,k,l}$ for every i, j, k, l.
5. Renew $V = V - \lambda V'$ and end if $\|V\|^2$ is sufficiently small, else go to 2.

After 20 iterations, we reconstructed the continuous approximation of V from these coefficients as

$$V(\vec{\mathbf{x}}) = \sum_{l=0}^{7} \sum_{i,j,k} c_{i,j,k,l}\psi_l(\vec{\mathbf{x}} - \vec{\mathbf{b}}_{i,j,k,l}). \tag{13}$$

Figure 2(c) is the same slice of the reconstructed volume as Figure 2(b). Figure 3(b) shows the difference between Figure 2(c) and 2(a). No visible difference indicates that sufficiently good expansion of V into 3D DOG functions was obtained.

We evaluated the same expansions by respectively using $\sigma_1 = 0.65$ and $\sigma_1 = 0.75$. Figure 4 shows the variations of the mean square errors between V and the reconstructed volumes as the number of iterations increases while changing the value of σ_1. Since the fastest convergence up to 20 iterations occurred at $\sigma_1 = 0.70$, hereafter we assume that $\sigma_1 = 0.70$.

5 Visualization of the DOG Representation

5.1 Reprojection of the Volume Density

The DOG representation can be visualized by simply reconstructing the discrete volume data from the equation (13) and then applying the conventional voxel based rendering technique [3, 4, 5]. Figure 5 is the example of the volume rendering [5] of the reconstructed voxels. However, reconstruction of the volume data is rather cumbersome for visualizing each primitive in order to analyze the multiresolutional structure of the volume. Since a 3D DOG function is considered to be a pair of Blinn's Blobby primitives as mentioned in **3**, equation (13) can be visualized in primitive order by depicting the implicit surface of a certain threshold value T [12] as

$$\sum_{l=0}^{7} \sum_{i,j,k} c_{i,j,k,l}\psi_l(\vec{\mathbf{x}} - \vec{\mathbf{b}}_{i,j,k,l}) = T.$$

However, this method needs tremendous rendering time and does not visualize the inside structure of the object.

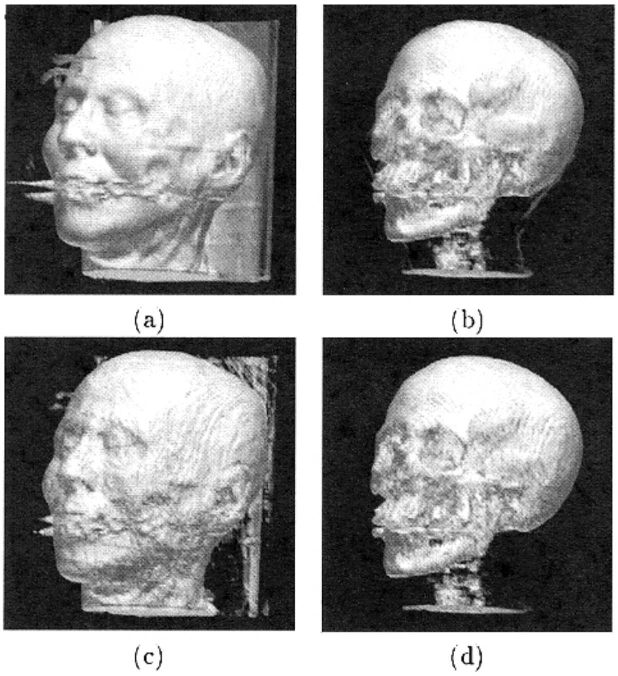

Figure 5: Comparison of the volume rendering images of the reconstructed volume data: (a),(b) All 2,971,734 primitives were used; (c),(d) The significant 136,346 primitives were used.

Then we propose the reprojection method[13, 14] which visualizes the inside structure of our 3D DOG representation without reconstructing the volume data. The reprojection method can be considered to be a ray casting method as illustrated in Figure 6(a). The irradiance of a pixel $\vec{\mathbf{p}}$ on the image plane, which is placed in front of the eye position $\vec{\mathbf{o}}$, is obtained by the integration of the densities of volume,

$$\int_{t_1}^{t_2} V(\vec{\mathbf{x}})dt = \sum_{l=0}^{7}\sum_{i,j,k} c_{i,j,k,l}\int_{t_1}^{t_2}\psi_l(\vec{\mathbf{x}}-\vec{\mathbf{b}}_{i,j,k,l})dt, \quad (14)$$

along the ray,

$$\vec{\mathbf{x}} = \vec{\mathbf{d}}t + \vec{\mathbf{o}},$$

where

$$\vec{\mathbf{d}} = \frac{\vec{\mathbf{p}}-\vec{\mathbf{o}}}{|\vec{\mathbf{p}}-\vec{\mathbf{o}}|}$$

denotes the unit direction vector of the ray. From Equation (5) and (8), Equation (14) is rewritten to

$$\int_{t_1}^{t_2} V(\vec{\mathbf{x}})dt$$

$$= \sum_{l=0}^{7}\sum_{i,j,k} 2^{-\frac{3}{2}l}c_{i,j,k,l}\{I(\vec{\mathbf{x}},\vec{\mathbf{b}}_{i,j,k,l},l,0.70)$$

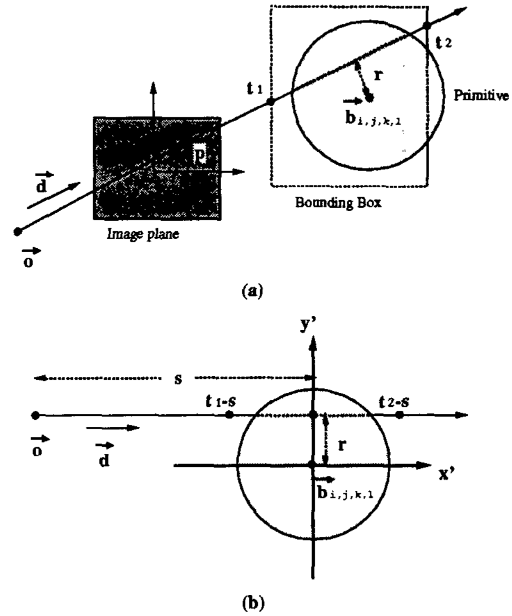

Figure 6: The volume density reprojection method.

$$- \left(\frac{1}{1.6}\right)^3 I(\vec{\mathbf{x}},\vec{\mathbf{b}}_{i,j,k,l},l,1.12)\}, \quad (15)$$

where

$$I(\vec{\mathbf{x}},\vec{\mathbf{b}}_{i,j,k,l},l,\sigma) = \int_{t_1}^{t_2} e^{-|\vec{\mathbf{x}}-\vec{\mathbf{b}}_{i,j,k,l}|^2/4^l\sigma^2}dt. \quad (16)$$

Since the integrand of Equation (16) is a spherically symmetric Gaussian function, which can be separated as Equation (11), Equation (16) is simplified to an 1D integral

$$I(\vec{\mathbf{x}},\vec{\mathbf{b}}_{i,j,k,l},l,\sigma) = e^{-r^2/4^l\sigma^2}\int_{t_1-s}^{t_2-s} e^{-x'^2/4^l\sigma^2}dx' \quad (17)$$

in a primitive centered coordinate system, $x'y'z'$, as illustrated in Figure 6(b). The integral of Equation (17) is further simplified to

$$\int_{t_1-s}^{t_2-s} e^{-x'^2/4^l\sigma^2}dx'$$

$$= 2^l\sigma\cdot\begin{cases}\{\mathrm{Erf}(\frac{t_2-s}{2^l\sigma})-\mathrm{Erf}(\frac{t_1-s}{2^l\sigma})\}, & s\le t_1\le t_2\\ \{\mathrm{Erf}(\frac{s-t_1}{2^l\sigma})+\mathrm{Erf}(\frac{t_2-s}{2^l\sigma})\}, & t_1\le s\le t_2\\ \{\mathrm{Erf}(\frac{s-t_1}{2^l\sigma})-\mathrm{Erf}(\frac{s-t_2}{2^l\sigma})\}, & t_1\le t_2\le s\end{cases}$$

where

$$\mathrm{Erf}(x) = \int_0^x e^{-t^2}dt$$

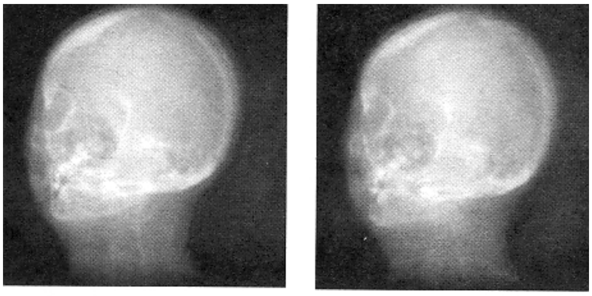

(a) $N = 2971734$ (b) $N = 136346$

Figure 7: Comparison of the reprojection images.

denotes the error function, which is included in the mathematical library of ordinary workstations, and s and r respectively denote

$$\begin{aligned} s &= (\vec{\mathbf{b}}_{i,j,k,l} - \vec{\mathbf{o}}) \cdot \vec{\mathbf{d}}, \\ r^2 &= \left|s\vec{\mathbf{d}} - (\vec{\mathbf{b}}_{i,j,k,l} - \vec{\mathbf{o}})\right|^2. \end{aligned}$$

By changing the extent of the integration, t_1 and t_2, we can visualize the arbitrary portion of the volume data. If we observe the entire volume data at a sufficient distance from the object, t_1 and t_2 are respectively considered to be $-\infty$ and ∞, then Equation (17) is still more simplified to

$$I(\vec{\mathbf{x}}, \vec{\mathbf{b}}_{i,j,k,l}, l, \sigma) = 2^l \sigma \sqrt{\pi} e^{-r^2/4^l \sigma^2}.$$

Figure 7(a) is the 256×256 reprojection image of the volume data by using all of the 2,971,734 primitives. Since the number of primitives N was so large, about 2 hours were required to render the image on an HP9000/735 workstation. However, most of the coefficients in Equation (15), $2^{-3l/2} c_{i,j,k,l}$, are negligible since the wavelet coefficients have significant values only where the volume density changes; furthermore, the human visual system is not sensitive at the higher spatial frequencies. Consequently, we can reduce the rendering time a great deal by using only the significant primitives. We used the primitives whose coefficients exceeded the threshold T_l, which was given to each scale, as

$$2^{-3l/2} c_{i,j,k,l} > T_l.$$

Figure 7(b) is the reprojection image of the volume data using the significant 136,346 primitives. The rendering time was reduced to 10 minutes and 18 seconds on the same workstation while maintaining the quality of the image. Table 1 shows the values of T_l and the numbers of the primitives N_l for each scale l.

Table 1: The threshold value T_l and the number of primitives N_l for each scale l.

l	T_l	N_l
0	400	109,737
1	300	19,086
2	200	6,119
3	200	1,123
4	200	188
5	100	65
6	50	24
7	25	4
Total		136,346

5.2 3D Edge Projection

Equation (14) sums up the primitives of all ls. Since our DOG function closely approximates a $\nabla^2 G$ function, the reprojection image for a particular l is almost equivalent to the 3D edge projection image of the scale. Figure 8 shows the 3D edge projection images on different scales. At the scale $l = 0$, fine structures such as the edges of bones or teeth are detected. The more the scale parameter l increases, the broader the detected structures are. This shows that our DOG representation consists of the hierarchy of an object's 3D edges on different scales.

We can obtain the edge enhanced images by defining the weight parameters

$$\mathbf{w} = (w_0, w_1, w_2, w_3, w_4, w_5, w_6, w_7),$$

and blending the 3D edge projection images on different scales as

$$\sum_{l=0}^{7} \sum_{i,j,k} w_l c_{i,j,k,l} \int_{t_1}^{t_2} \psi_l(\vec{\mathbf{x}} - \vec{\mathbf{b}}_{i,j,k,l}) dt.$$

Figure 9(a) is an edge enhanced image rendered by using $\mathbf{w} = (4, 3, 2, 1, 1, 1, 1, 1)$. In contrast to Figure 7(b), which corresponds to $\mathbf{w} = (1, 1, 1, 1, 1, 1, 1, 1)$, it is clearly shown that the 3D structures of higher frequencies are enhanced. Although the frequency domain volume rendering methods [16, 17] generate similar edge enhanced images, our method is suitable for the partial enhancement of the edge information. Figure 9(b) is an edge enhanced image rendered by using a bounding box which is smaller than the size of the head. Figure 9(c) is the blended image of Figure 7(b) and 9(b). In this manner, we can enhance the arbitrary portion of the volume data.

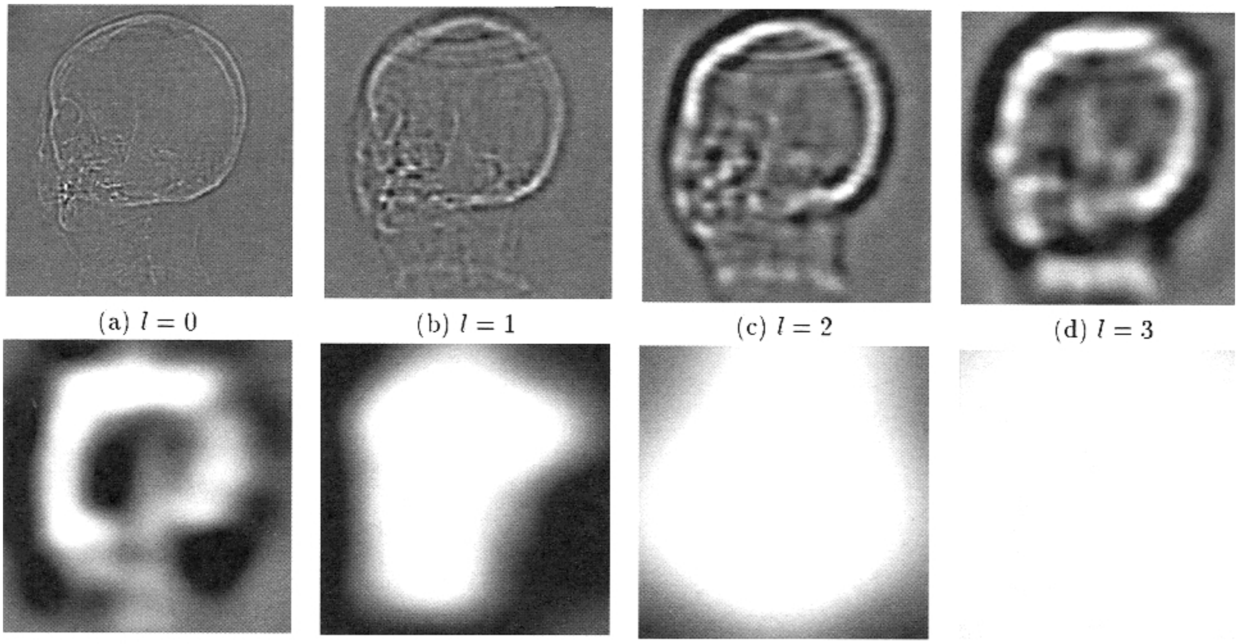

(a) $l = 0$ (b) $l = 1$ (c) $l = 2$ (d) $l = 3$

(e) $l = 4$ (f) $l = 5$ (g) $l = 6$ (h) $l = 7$

Figure 8: The 3D edge projection images on different scale.

6 Conclusions

We have proposed a volume representation method by expanding volume data into 3D DOG primitives. Because of the feature of the 3D Gaussian functions, the perspective projection of our volume representation was calculated much easier than that of the conventional voxel representation. Specifically, our method describes the volume by spherically symmetric continuous functions, so we do not need to be concerned with either the directions or the discontinuities which arise from the cubic shapes of the voxels. By neglecting the insignificant coefficients, we were able to reduce the number of primitives a great deal without spoiling the quality of the reprojection image. Also, since the DOG function approximates a $\nabla^2 G$ function, we were able to enhance the 3D edge information at will by simply adjusting the weight parameter which was given to each scale. We can expect to use this enhancement for medical diagnostics. Further, since we were able to construct the 3D wavelets by the pair of spherically symmetric functions, we may also expect to use this method for the automatic generation of Blinn's blobby objects [15] and other blobby objects, such as metaballs [18] and soft objects [19]. Since the wavelets have no DC components in general, the average value of the reconstructed volume reduces to zero. This problem may be avoided by approximating the volume by a single function, e.g. Gaussian, in advance and then expanding the rest of the volume by the wavelets.

Although the DOG representation simplified the projection calculations of the volume densities, the rendering times were still long compared with conventional voxel based methods. To reduce the rendering time, we may use the *splatting method* [20] in an orthographic view. In our representation the *footprint* will become circularly symmetric and invariant to the object's rotation, therefore we only need to prepare several footprints for different scales in advance. Parallelism of our method may also be possible. We can apply both pixelwise and primitivewise parallelism. We look forward to our method being comparable to the voxel representation in terms of rendering speed.

References

[1] Udupa, Jayaram K. and Gabor T. Herman, 3D Imaging in Medicine, CRC Press, 1991.

[2] Kaufman, Arie, Volume Visualization, IEEE Computer Society Press, 1991.

[3] Lorensen, William E. and Harvey E. Cline, Marching Cubes: A High Resolution 3D Surface Construction Algorithm, Proceedings of SIG-

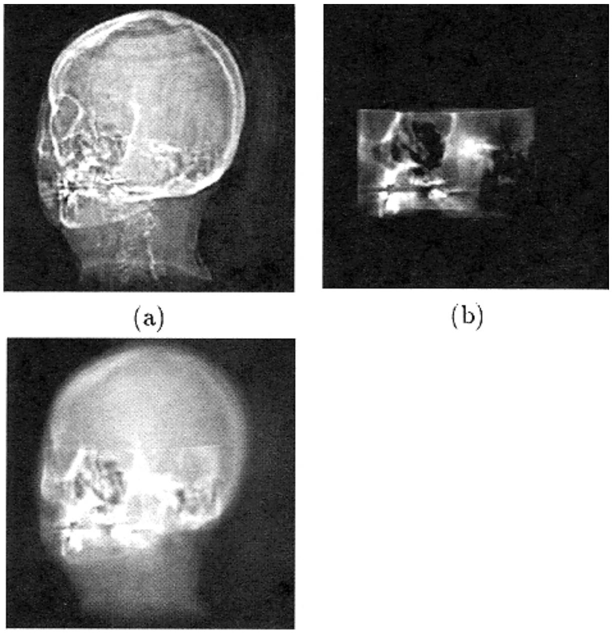

(a) (b)

(c)

Figure 9: A few examples of the 3D edge enhancements.

GRAPH'87 (Anaheim, California, uly 27-31, 1987). In *Computer Graphics* Vol.21, No.4 (July 1987), pp. 163-169, 1987

[4] Drebin, Robert A., Loren Carpenter and Pat Hanrahan, Volume Rendering, Proceedings of SIGGRAPH'88 (Atlanta, Georgia, August 1-5, 1988). In *Computer Graphics*, Vol.22, No.4, pp. 51-58, 1988.

[5] Levoy, Mark, Display of Surface from Volume Data, *IEEE CG&A*, Vol.8, No.5, pp. 29-37, 1988.

[6] Marr, David and E. Hildreth, Theory of edge detection, Proc. R. Soc. London, B 207, pp187-217, 1980.

[7] Daubechies, Ingrid, Ten Lectures on Wavelets, SIAM CBMS-61, 1992.

[8] Mallat, Stephane G., A Theory for Multiresolution Signal Decomposition: The Wavelet Representation, *IEEE Trans. PAMI*, Vol.11, No.7, pp.674-693, 1989.

[9] Muraki, Shigeru, Volume Data and Wavelet Transforms, *IEEE CG&A*, Vol.13, No.4, pp.50-56, 1993.

[10] Murenzi, R., Wavelet Transforms Associated to the n-Dimensional Euclidean Group with Dilations: Signal in More Than One Dimension, In Wavelets, J.M. Combes, A. Grossmann, and Ph. Tchamitchian, eds., Springer-Verlag, Berlin, pp. 239-246, 1989.

[11] Blinn, James F., A Generalization of Algebraic Surface Drawing, *ACM Trans. on Graphics*, Vol.1, No.3, pp.235-256, 1982.

[12] Kalra, Devendra and Alan .H. Barr, Guaranteed Ray Intersections with Implicit Surfaces, Proceedings of SIGGRAPH'89 (Boston, Massachusetts, July 31-August 4, 1989). In *Computer Graphics*,, Vol.23, No.3, pp. 297-306, 1989.

[13] Harris, L. D., R. A. Robb and E. L. Ritman, Visual enhancement and display of three-dimensional reconstructed anatomic morphology, *Proc. 6th CCAR*, pp. 278-284, 1979.

[14] Jin, Xiuyi, Mitsuhide Kimura, Shigeki Yokoi, Junichiro Toriwaki and Michimasa Matsuo, A Computer Aided Diagnosis System Based on 3D Density Reprojection Methods, *Japanese Journal of Medical Electronics and Biological Engineering* , Vol.27, No.3, pp. 127-133, 1989. (In Japanese.)

[15] Muraki, Shigeru, Volumetric Shape Description of Range Data using "Blobby Model", Proceedings of SIGGRAPH'91 (Las Vegas, Nevada, July 29-August 2, 1991). In *Computer Graphics*, Vol.25, No.4, pp. 227-235, 1991.

[16] Malzbender, Tom, Fourier Volume Rendering, *ACM Transactions on Graphics*, Vol.12, No.3, July 1993.

[17] Totsuka, Takashi and Marc Levoy, Frequency Domain Volume Rendering, Proceedings of SIIGGRAPH'93 (Anaheim, California, August 1-6, 1993). In *Computer Graphics* Proceedings, Annual Conference Series, 1993, ACM SIGGRAPH, New York, 1993, pp.271-278.

[18] Nishimura, Hitoshi, Makoto Hirai, Toshiyuki Kawai, Toru Kawata, Isao Shirakawa and Koichi Ohmura, Object Modeling by Distribution Function and a Method of Image Generation, *Trans. IEICE Japan*, Vol.J68-D, No.4, pp.718-725, 1985. (In Japanese.)

[19] Wyvill, Geoff, C. McPheeters and Brian Wyvill, Data Structure for Soft Objects, *The Visual Computer*, Vol.2, pp.227-234, 1986.

[20] Westover, Lee, Footprint Evaluation for Volume Rendering, Proceedings of SIGGRAPH'90 (Dallas, Texas, August 6-10, 1990). In *Computer Graphics*, Vol.24, No.4, pp. 367-376, 1990.